A Bidirectional Integrated Equalizer Based on the Sepic–Zeta Converter for Hybrid Energy Storage System

Bin Xu, *Student Member, IEEE*, Zhaotian Yan, Wei Zhou, *Member, IEEE*, Lu Zhang, Huazhong Yang, *Fellow, IEEE*, Yongpan Liu, *Senior Member, IEEE*, and Lizhou Liu, *Member, IEEE*

***Abstract*—In the hybrid energy storage system (HESS), the voltages between the battery cell and the supercapacitor cell are different, increasing the circuit and control complexity of the balance system. Therefore, a bidirectional integrated equalizer based on the Sepic–Zeta converter is proposed for the HESS, which realizes both battery string and supercapacitor string balance during the energy exchange. The inductors in the Sepic–Zeta converter are used as the primary side of the balanced multiwinding transformer. The Sepic–Zeta converter generates the current ripples to drive the multiwinding transformer. The secondary side generates currents to balance the HESS, and hence, the equalizer itself is essentially switchless. Therefore, the proposed circuit can reduce the complexity of the HESS. Experimental and comparative results show that the proposed equalizer achieves the balance of the HESS.**

***Index Terms*—Battery management system, cell balancing, current ripple, multiwinding transformer.**

I. Introduction

THE hybrid energy storage system (HESS) generally comprises the battery strings and supercapacitor strings [1], [2]. Supercapacitor auxiliary battery work, making the HESS, has the advantages of high-energy density and high-power density, and it can prolong the life of the battery string [3]. However, both the supercapacitor string and battery string consist of series-connected energy storage monomers, which lead to an imbalance of cells voltage. However, both the supercapacitor and battery strings consist of series-connected energy storage monomers, leading to an imbalance of cell voltage [4], [5]. Due to "barrel effects," the actual storage capacity of the energy storage system (ESS) is determined by the highest voltage cell and the lowest voltage cell [6]. The unbalance of the HESS may decrease the capacity and even threaten the safety of the HESS [7]. Thus, it is necessary to integrate the balance circuit into the HESS.

The existing equalizers can be mainly divided into passive balance methods and active balance methods. The passive balance method uses a resistor in parallel with each battery, and the current is bypassed from the cells to balance the cell's voltages. This balancing method is low-cost and easy to implement without any control. However, the passive balance method is inefficient, and heat dissipation problems occur. Compared with the energy dissipation methods, the active balance methods use electronic components to transfer more energy to low-voltage batteries [8]. According to the classification of electronic components, the active balance method can be divided into switch-capacitor-based [9]–[15], inductor-based [16], [17], transformer-based [18]–[25], voltage multiplier [26]–[31], and switch matrix [32], [33].

Compared with another equalizer, the multiwinding-transformer-based equalizer has the advantage of electrical isolation and simple control. Chen *et al.* [18] proposed a balanced structure based on a forward and flyback transformer. The structure transfers energy to adjacent batteries through the forward transformer and transfers the residual magnetism in the magnetic core to the remaining batteries through the flyback converter. The circuit structure passes the flyback converter and simplifies the system complexity. It is worth mentioning that Shang *et al.* [19] designed a series of high-efficiency compact equalizers with simple control based on switched-capacitor or forward–flyback converters. The equalizer uses a secondary winding to connect two battery strings, and the energy can be directly flowed from a high-voltage battery to a low-voltage battery through the secondary winding to achieve battery balance. At the same time, this equalizer requires only one switch for each battery cell. A unitized multiwinding-transformer-based equalization method is proposed [22]. The forward converter and flyback converter are realized simultaneously. The forward converter principle is used to equalize the battery cells in the same subunit, while the flyback converter principle is applied to equalize the different subunits. Therefore, fewer metal-oxide-semiconductor field-effect transistors (MOSFET) and transformer windings are needed for lower control complexity and lower system cost.

Manuscript received December 2, 2021; revised February 8, 2022; accepted March 18, 2022. Date of publication March 24, 2022; date of current version June 24, 2022. This work was supported in part by the National Key Research and Development Program under Grant 2018YFA0701500, in part by the NSFC under Grant 62106125, and in part by the Cultivation Program for the Excellent Doctoral Dissertation of Southwest Jiaotong University under Grant 2020YBPY06. Recommended for publication by Associate Editor G. Oriti. *(Bin Xu and Zhaotian Yan contributed equally to this work.) (Corresponding author: Lizhou Liu.)*

Bin Xu, Zhaotian Yan, and Wei Zhou are with the School of Electrical Engineering, Southwest Jiaotong University, Chengdu 610031, China (e-mail: xubin@my.swjtu.edu.cn; zhaotian_yan@163.com; wzhou@swjtu.edu.cn).

Lu Zhang, Huazhong Yang, Yongpan Liu, and Lizhou Liu are with the School of Electronic Engineering, Tsinghua University, Beijing 10086, China (e-mail: willvsnick@tsinghua.edu.cn; yanghz@tsinghua.edu.cn; ypliu@tsinghua.edu.cn; liulizhou@163.com).

Color versions of one or more figures in this article are available at https://doi.org/10.1109/TPEL.2022.3161984.

Digital Object Identifier 10.1109/TPEL.2022.3161984

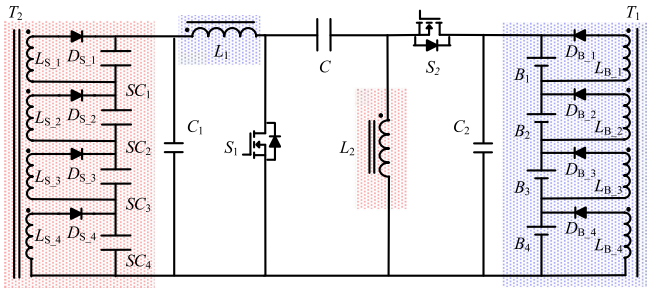

Fig. 1. Structure of the proposed equalizer for four batteries and supercapacitors.

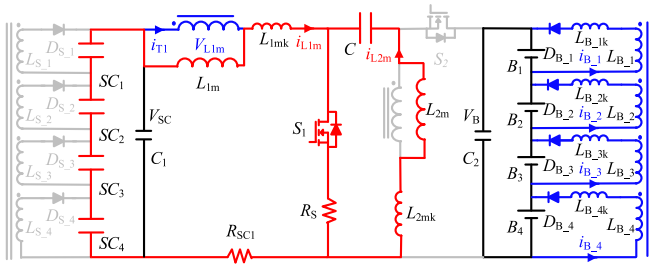

Fig. 2. Operating state of the proposed equalizer in the SSC state I.

Any-cell-to-any-cell equalizer based on coupled half-bridge converters is proposed [25], which reduces the transformer windings by half and achieves a compact size and low cost. Furthermore, realizing the automatic any-cell-to-any-cell equalization speeds up the equalization process.

The methods mentioned above are externally added to the ESS, and the dc–dc converter and equalizer operate individually. It means that the ESS needs the functional components of the dc–dc converter and equalizer, respectively [28]. An integrated charging equalizer based on the buck–boost converter (ICEBC) is proposed [24]. The current ripple drives the multiwinding transformer to balance the battery string. The ICEBC can realize the automatic equalization without extra switches. A tapped inductor (TI)-based single magnetic bidirectional PWM converter integrating a voltage equalizer for series-connected supercapacitors is proposed [29]. The TI plays three roles in the proposed integrated converter. Magnetizing and leakage inductances are utilized as filter inductors and sonant inductors, respectively. The resonant voltage multiplier is driven by the square wave voltage generated by the TI. However, all balancing current will flow through the battery closest to the negative pole, resulting in a large current on the cell. Therefore, the TI-based voltage equalizer is more suitable for supercapacitor strings as voltage equalization. In the HESS, due to the different voltages of the battery cells and the supercapacitor cells, at least two sets of equalization devices are required, resulting in extra electronic components and high costs.

Therefore, a charging equalizer based on the bidirectional Sepic–Zeta converter is proposed for the HESS, which realizes the balance function of the HESS in the process of energy exchange. The inductances in the Sepic–Zeta converter are used as the primary side of the multiwinding transformers. And the current ripple drives the multiwinding transformer, so the equalizer itself is essentially switchless. The proposed circuit can reduce the complexity of the HESS. Finally, a series of experiments are conducted to confirm the effectiveness of the proposed topology.

II. Proposed Equalizer

A. Configuration of the Equalizer

As shown in Fig. 1, the proposed topology includes the bidirectional Sepic–Zeta converter and multiwilding transformers. When the supercapacitor string charges the battery string, the inductor L_1 works to balance the supercapacitor string, and the inductor L_2 works to balance the supercapacitor string. When the battery string charges the supercapacitor string, the inductor L_1 works to balance the battery string, and the inductor L_2 works to balance the supercapacitor string. The voltage of the supercapacitor is $V_{\rm SC}$ and the voltage of the battery string is $V_{\rm B}$.

In order to simplify the circuit analysis, the parameters in the circuit are assumed as follows:

1) $L_{\rm im}$ represents the magnetizing inductances of the L_i. L_{imk} represents the leakage inductance of the primary side. L_{B_i} and L_{B_ik} ($i = 1, 2, 3, 4$) represent the magnetizing inductance and the leakage inductances on a secondary winding for battery string, respectively. L_{S_i} and L_{S_ik} are the magnetizing inductance and the leakage inductances on a secondary winding for supercapacitor string, respectively. D_{B_i} and D_{S_i} are the diodes on a secondary winding, and the diode forward voltage drops of the D_{B_i} and D_{S_i} are V_{DB} and V_{DS}, respectively. And the multiwinding transformer can be seen as an ideal transformer.
2) N_{11} and N_{12} represent the turns of the primary windings and the secondary windings in the transformer T_1. N_1 is the turn ratio of the transformer, expressed as $N_1 = N_{11}/N_{12}$. N_{21} and N_{22} represent the turns of the primary windings and the secondary windings in the transformer T_2, respectively. N_2 is the turn ratio of the transformer, expressed as $N_2 = N_{21}/N_{22}$. Assume that T_1 and T_2 are ideal transformers. The current flowing through the transformer T_1 is i_{T1}, and the current flowing through the transformer T_2 is i_{T2}. The switching frequency is f.
3) The relationship among the battery cell voltages is $VB\_1 > VB\_2 > VB\_3 > VB\_4$. And the supercapacitor cell voltages are $VS\_1 > VSC\_2 > VSC\_3 > VSC\_4$.

B. Supercapacitor String Charging (SSC) Mode

The supercapacitor string charges the battery string. In one cycle period, the proposed circuit has two states.

State I ($t_0 - t_1$): At t_0, the S_1 turns ON, and the supercapacitor string charges the inductor L_1 through S_1. The current i_{T1} rises and the secondary side of T_1 generates current to balance the battery cells. The transfer capacitor C transfers the energy to L_2 through S_1. The current i_{L2m} is opposite the transformer T_2, so T_2 does not work. In state I, the operating state of the proposed circuit is shown in Fig. 2.

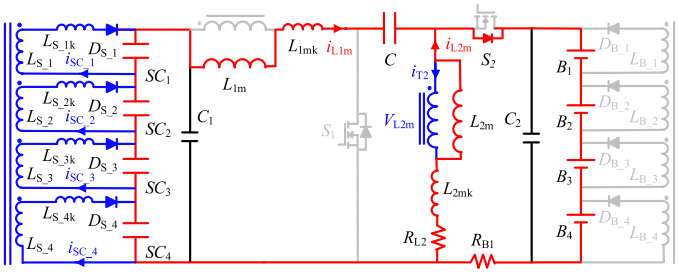

Fig. 3. Operating state of the proposed equalizer in the SSC state II.

The equivalent resistance of the supercapacitor string and L_1 can be derived as

$$R_{\mathrm{SC1}} = R_{\mathrm{SC}} + R_{L1} \tag{1}$$

where R_{SC} is the internal resistance of the supercapacitor string. R_{L1} is the internal resistance of L_1.

The voltages of inductor L_{1m} is

$$V_{L1m} = V_{\mathrm{SC}} - L_{1\mathrm{mk}} \cdot \frac{di_{L1m}}{dt} - (R_{\mathrm{SC1}} + R_{\mathrm{S}}) \cdot i_{L1m} \tag{2}$$

where V_{L1m} is the voltage of L_{1m}. L_{1mk} is the leakage inductance of L_{1m}. R_S is the internal resistance of S_1.

When the voltage of the secondary winding L_{B_i} is V_{LB_i}, which is higher than battery voltage V_{B_i}, the balance current will be formed in the secondary loop. The relationship between V_{LB_i} and i_{B_i} can be derived as

$$V_{LB\_i} = V_{B\_i} + L_{B\_ik} \cdot \frac{di_{B\_i}}{dt} + V_{DB} + R_{B\_i} \cdot i_{B\_i} \tag{3}$$

where R_{B_i} respects the internal resistance in the secondary winding loop. i_{B_i} is the balance current of B_i.

The relationship between the voltage on the primary winding and the voltage on the secondary winding satisfies

$$\frac{V_{L1m}}{V_{LB\_i}} = \frac{N_{11}}{N_{12}} = N_1. \tag{4}$$

The battery balance current i_{B_i} satisfies

$$i_{B\_i}(\mathrm{t}) = \frac{V_{LB\_i} - V_{B\_i} - V_{DB}}{L_{B\_ik}} \cdot (t - t_0)\,. \tag{5}$$

From (5), the factors that determine the balance current i_{B_i} include the voltage of supercapacitor string, turns ratio N_1, and V_{B_i}. Due to the winding ratio of the secondary windings of the multiwinding transformer is the same, the equalizing current of the low-voltage battery is larger and the equalizing current of the high-voltage battery is smaller.

State II ($t_1 - t_2$): At t_1, the S_1 turns OFF. The supercapacitor string and the inductor L_1 charge the transfer capacitor C and the battery string through the body diode of S_2. The inductor L_1 releases the energy, which can demagnetize. The inductor L_2 charges the battery string through the body diode of S_2. The current i_{T2} rises and the secondary side of T_2 generates current to balance the supercapacitor cells. In state II, the operating state of the proposed circuit is shown in Fig. 3.

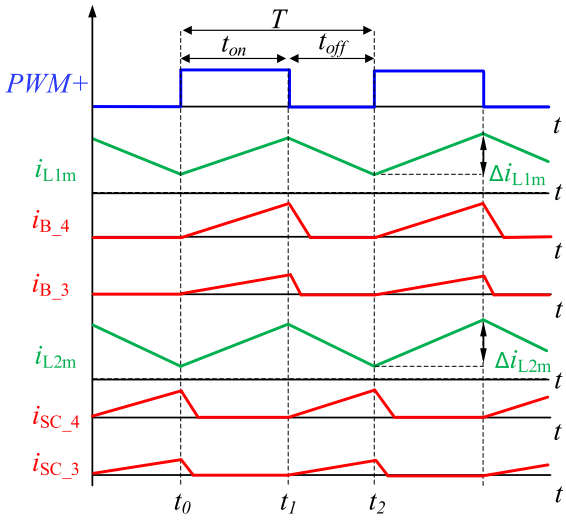

Fig. 4. Key waveforms of the proposed equalizer.

The equivalent resistance of the battery string and S_2 can be derived as

$$R_{B1} = R_{SD} + R_B \tag{6}$$

where R_{SD} is the internal resistance of S_2's body diode. R_B is the internal resistance of the battery string.

The terminal voltage of the primary winding of the ideal transformer satisfies

$$V_{L2m} = V_B + L_{2mk} \cdot \frac{di_{L2m}}{dt} + (R_{B1} + R_{L2}) \cdot i_{L2m} \tag{7}$$

where R_{L2} is the internal resistance of L_2.

The relationship between V_{LS_i} and $i_{\_\mathrm{SC}i}$ can be expressed as

$$V_{\mathrm{LS\_}i} = V_{\mathrm{SC\_}i} + L_{S\_ik} \cdot \frac{di_{\mathrm{SC\_}i}}{dt} + V_{DS} + R_{\mathrm{SC\_}i} \cdot i_{\mathrm{SC\_}i} \tag{8}$$

where $R_{\_\mathrm{SC}i}$ respects the internal resistance in secondary winding loop. $i_{\_\mathrm{SC}i}$ respects the balance current of SC_i. V_{LS_i} is the voltage of the L_{S_i}.

The relationship between the voltage on the primary winding and the voltage on the secondary winding satisfies

$$\frac{V_{L2m}}{V_{LS\_i}} = \frac{N_{21}}{N_{22}} = N_2. \tag{9}$$

The battery balance current $i_{\_\mathrm{SC}i}$ satisfies

$$i_{\mathrm{SC\_}i}(\mathrm{t}) \frac{V_{LS\_i} - V_{\mathrm{SC\_}i} - V_{DS}}{L_{S\_ik}} \cdot (t - t_1)\,. \tag{10}$$

The key waveforms of the proposed equalizer are shown in Fig. 4. Due to $V_{B\_3} > V_{B\_4}$, i_{B_3} is smaller than i_{B_4}, and $V_{\_\mathrm{SC3}} > V_{\_\mathrm{SC4}}$, $i_{\_\mathrm{SC3}}$ is smaller than $i_{\_\mathrm{SC4}}$. It proves that the voltage equalizer can balance the HESS by transformers.

C. Battery String Charging (BSC) Mode

The battery string charges the supercapacitor string. In one cycle period, the proposed circuit has two states.

State I ($t_0 - t_1$): At t_0, the S_2 turns ON. The battery string charges the inductor L_2 through S_2. The current i_{T2} rises and

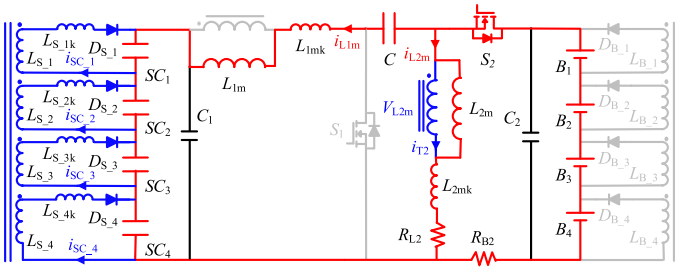

Fig. 5. Operating state of the proposed equalizer in the BSC state I.

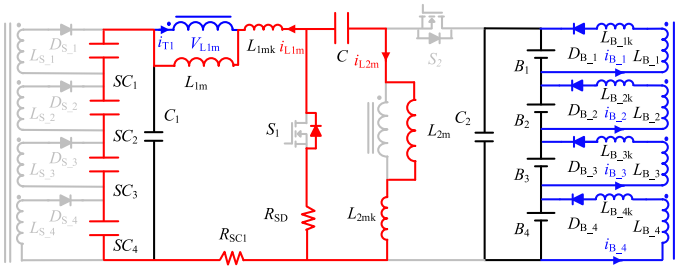

Fig. 6. Operating state of the proposed equalizer in the BSC state II.

the secondary side of T_2 generates current to balance the supercapacitor cells. The battery string and the transfer capacitor C charge the inductor L_1 and the supercapacitor string through S_2. In state I, the operating state of the proposed circuit is shown Fig. 5.

The equivalent resistance of the S_2 and battery string can be derived as

$$R_{B2} = R_S + R_B \tag{11}$$

where R_S is the internal resistance of S_2.

The voltage V_{L2m} can be expressed as

$$V_{L2m} = V_B - L_{2mk} \cdot \frac{di_{L2m}}{dt} - (R_{B2} + R_{L2}) \cdot i_{L2m}. \tag{12}$$

The relationship between $V_{\_\mathrm{SC}i}$ and $i_{\_\mathrm{SC}i}$ can be expressed as

$$V_{\mathrm{LS}\_i} = V_{\mathrm{SC}\_i} + L_{S\_ik} \cdot \frac{di_{\mathrm{SC}\_i}}{dt} + V_{DS} + R_{\mathrm{SC}\_i} \cdot i_{\mathrm{SC}\_i}. \tag{13}$$

The battery balance current i_{B_i} satisfies

$$i_{B\_i}(\mathrm{t}) \frac{V_{\mathrm{LS}\_i} - V_{\mathrm{SC}\_i} - V_{DS}}{L_{S\_ik}} \cdot (t - t_0)\,. \tag{14}$$

The relationship between the voltage on the primary winding and the voltage on the secondary winding satisfies

$$\frac{V_{L2m}}{V_{\mathrm{LS}\_i}} = \frac{N_{21}}{N_{22}} = N_2. \tag{15}$$

State II (t_1 – t_2): At t_1, the S_2 turns OFF. The inductor L_2 charges the transfer capacitor C through the body diode of S_1. The inductor L_1 charges the supercapacitor string through the body diode of S_1. The current i_{T1} rises and the secondary side of T_1 generates current to balance the battery cells. In state II, the operating state of the proposed circuit is shown Fig. 6.

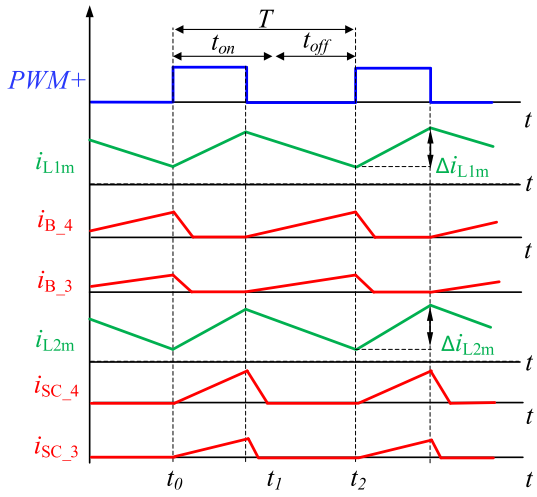

Fig. 7. Key waveforms of the proposed equalizer.

The voltage V_{L1m} can be expressed as

$$V_{L1m} = V_{\mathrm{SC}} + L_{1mk} \cdot \frac{di_{L1m}}{dt} + (R_{\mathrm{SC1}} + R_{\mathrm{SD}}) \cdot i_{L1m} \tag{16}$$

where R_{SD} is the internal resistance of S_1's body diode.

The relationship between V_{B_i} and i_{B_i} can be derived as

$$V_{LB\_i} = V_{B\_i} + L_{B\_ik} \cdot \frac{di_{B\_i}}{dt} + V_{DB} + R_{B\_i} \cdot i_{B\_i}. \tag{17}$$

The battery balance current i_{B_i} satisfies

$$i_{B\_i}(\mathrm{t}) \frac{V_{LB\_i} - V_{B\_i} - V_{DB}}{L_{B\_ik}} \cdot (t - t_1)\,. \tag{18}$$

The key waveforms of the proposed equalizer are shown in Fig. 7. Due to $V_{B\_3} > V_{B\_4}$, i_{B_3} is smaller than i_{B_4}, and $V_{\_\mathrm{SC3}} > V_{\_\mathrm{SC4}}$, $i_{\_\mathrm{SC3}}$ is smaller than $i_{\_\mathrm{SC4}}$. It proves that the voltage equalizer can balance the HESS by transformers.

III. Design of the System

A. Design the Turn Ratio

1) In SSC Mode: Turn ratio N_1: The actual current I_{Bi_al} flowing through the battery B_i can be expressed as

$$I_{Bi\_al} = I_{B\_i} + I_B \tag{19}$$

where I_{B_i} is the average balancing current of the B_i and I_B is the charging current of the battery string.

From (5), I_{B_i} can be derived as

$$\begin{aligned} I_{B\_i} &= \frac{1}{T} \int_0^{DT} \frac{t \cdot \left(\frac{V_{L1m}}{N_1} - V_{B\_i} - V_{DB}\right)}{L_{B\_ik}} dt \\ &= \frac{\left(\frac{V_{L1m}}{N_1} - V_{B\_i} - V_{DB}\right)}{2f \cdot L_{B\_ik}} D^2 \end{aligned} \tag{20}$$

where T is the time of one switching cycle.

From (20), the minimum value of turn ratio N_1 can be expressed as

$$N_1 \geq \frac{V_{L1m}}{\frac{2f \cdot L_{B\_ik} \cdot I_{B\_i\_\max}}{D^2} + V_{B\_i} + V_{BD}} \tag{21}$$

where $I_{B\_i\_\max}$ is the maximum value of balance current.

The battery balancing currents mainly depend on the voltage of supercapacitor string $V_{\rm SC}$, duty cycle D, and operating frequency f.

To ensure that the proposed circuit has the balancing function.The maximum value of turn ratio N_1 can be expressed as

$$N_1 < \frac{V_{L1m}}{V_{B\_i\_\min} + V_{BD}} \tag{22}$$

where $V_{B\_i\_\min}$ is the minimum voltage of battery cell.

Turn ratio N_2:

From (10), the average balancing current $I_{\_{\rm SC}i}$ can be expressed as

$$\begin{aligned} I_{\rm SC\_}i &= \frac{1}{T}\int_0^{DT} \frac{t \cdot \left(\frac{V_{L2m}}{N_2} - V_{\rm SC\_}i - V_{DS}\right)}{L_{S\_ik}} dt \\ &= \frac{\frac{V_{L2m}}{N_2} - V_{\rm SC\_}i - V_{DS}}{2f \cdot L_{S\_ik}} D^2. \end{aligned} \tag{23}$$

Due to the high-power density of supercapacitors, there is no need to consider the current threshold. The winding range of N_2 is

$$N_2 = \frac{V_{L2m}}{V_{\rm SC\_}i\_\max + V_{DS}}. \tag{24}$$

When the battery voltage V_{L2m} is maximum, the voltage of supercapacitor is cell equal to threshold.

2) In BSC Mode: The design method of turn ratio is the same as the SSC mode.

B. Design the Parameters of Inductor/Capacitor

1) Design of the Inductor: When the S_1 turns ON, the value of inductor L_1 can be expressed as

$$L_1 = \frac{V_{\rm SC} D}{\Delta i_{L1m} f} \tag{25}$$

where Δi_{L1m} is the current ripple of i_{L1m}.

When the S_1 turns OFF, the value of inductor L_1 can be derived as

$$L_2 = \frac{V_B (1 - D)}{\Delta i_{L2m} f} \tag{26}$$

where Δi_{L2m} is the current ripple of i_{L2m}.

2) Design of the Stabilizing Capacitor: C_1 and C_2 are voltage stabilizing capacitors, and the capacitance value is designed based on the output current. The charge calculation formula for the capacitance can be expressed as

$$Q = \frac{I_{\rm out}}{f} \tag{27}$$

where Q is the electric charge and $I_{\rm out}$ is the output current.

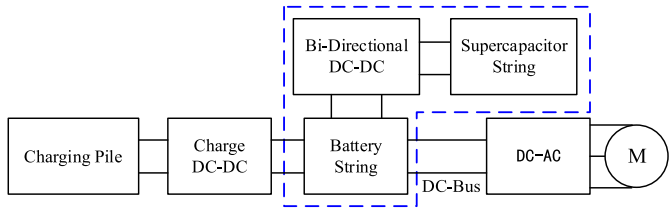

Fig. 8. Circuit structure of proposed.

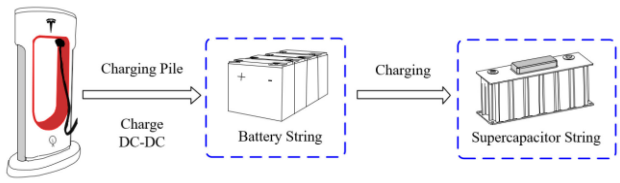

Fig. 9. State of the HESS in charging process.

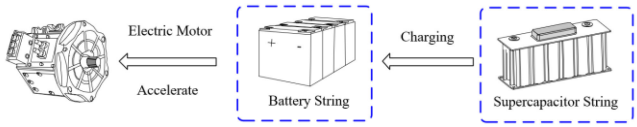

Fig. 10. State of the HESS in discharging process.

The capacitance of a capacitor can be derived as

$$C = \frac{Q}{\Delta u} \tag{28}$$

where Δu is the maximum voltage fluctuation.

3) Design of the Transfer Capacitor: C is the transfer capacitor, and the capacitance value is designed based on the output current. The voltage ripple ΔV_C of the transfer capacitor terminal can be expressed as

$$C = \frac{\Delta Q}{\Delta V_C} = \frac{I_{\rm av}}{\Delta V_C \cdot f} \tag{29}$$

where $I_{\rm av}$ is the average current flowing through the transfer capacitor C in one cycle.

C. Control of Proposed Circuit

The proposed charging equalizer for the HESS is shown in Fig. 8. The charging pile charges the battery string through dc–dc. The battery string is directly connected to the dc bus, and the supercapacitor string is connected to the battery string through the proposed circuit.

Take the application scenario of electric vehicles (EV) as an example. When the EV is charging, the battery string charges the supercapacitor string, as shown in Fig. 9.

When the EV is accelerated, the supercapacitor string charges the battery string, as shown in Fig. 10.

1) The SSC mode: Upercapacitor string transfers energy to the battery string. The battery string adopts a constant current (CC)–constant voltage (CV) charging method. The voltage V_B and the output current I_B are feedbacked to control the duty cycle of S_1, as shown in Fig. 11.

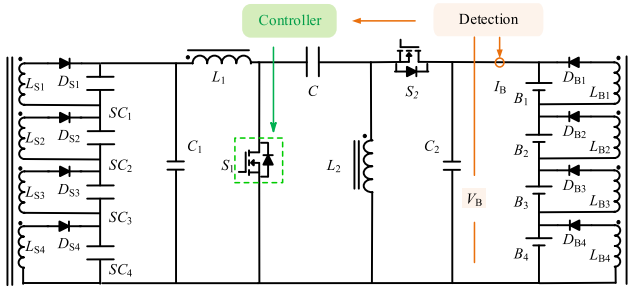

Fig. 11. Control method of the proposed converter in the SSC mode.

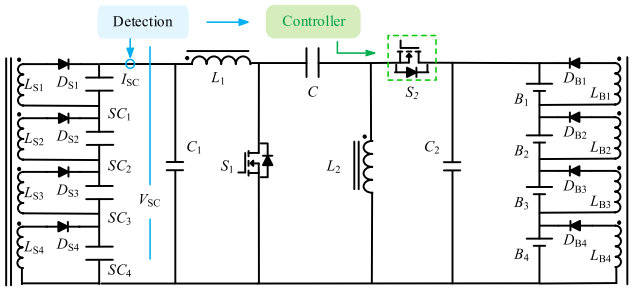

Fig. 12. Control method of the proposed converter in the BSC mode.

2) The BSC mode: The battery string transfers energy to the supercapacitor string. The supercapacitor string adopts the CC–CV charging method. The voltage $V_{\rm SC}$ and the output current $I_{\rm SC}$ are feedbacked to control the duty cycle of S_2, as shown in Fig. 12.

D. Systems' Efficiency

Generally, the balance systems' efficiency can be divided into the SSC mode $\eta_{\rm SC}$ and the BSC mode η_B

$$\eta_{\rm SC} = \frac{V_B I_B + \sum_{i=1}^{n} I_{B\_i} \cdot V_{B\_i}}{V_{\rm SC} I_{\rm SC} - \sum_{j=1}^{m} I_{{\rm SC}\_j} \cdot V_{{\rm SC}\_j}}$$
$$\eta_B = \frac{V_{\rm SC} I_{\rm SC} + \sum_{j=1}^{m} I_{{\rm SC}\_j} \cdot V_{{\rm SC}\_j}}{V_B I_B - \sum_{i=1}^{n} I_{B\_i} \cdot V_{B\_i}} \tag{30}$$

where I_B is the current of the battery string. $I_{\rm SC}$ is the current of the supercapacitor string. n and m are the cell number of the battery and supercapacitor strings, respectively.

The bypass resistance loss $P_{\rm pass}$ can be expressed as

$$P_{\rm pass} = \sum_{j=1}^{m} I_{{\rm SC}\_j}^2 R_{{\rm SC}\_j} + \sum_{i=1}^{n} I_{B\_i}^2 R_{B\_i} + I_{\rm av}^2 R_P \tag{31}$$

where R_P is the conduct resistance of the bidirectional converter circuit.

The diode voltage drop loss P_D can be expressed as

$$P_D = \sum_{j=1}^{m} I_{{\rm SC}\_j} V_{DS} + \sum_{i=1}^{n} I_{B\_i} V_{DB} + I_{\rm av} V_D \tag{32}$$

where V_D is the diode forward voltage drops of S_1's (S_2) body diode.

The switching loss consists of three sides P_c, P_s, and $P_{\rm DC}$. P_c is the conducting losses of the switch; P_s is the switching losses. $P_{\rm DC}$ is the drive circuit loss. R_{DS}, $E_{\rm OFF}$, $E_{\rm ON}$, U_{DD}, I_D, Q_{RR}, U_{DD}, I_D, and I_{R_D} are some inherent parameters of the MOSFET, which can be found or fitted in the MOSFET's datasheet.

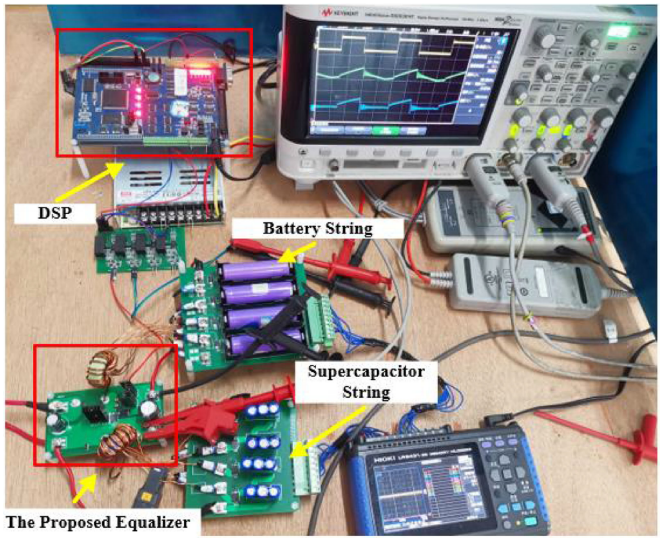

Fig. 13. Photograph of the experimental setup and associated instruments.

TABLE I
SPECIFICATIONS OF THE TRANSFORMER

Symbol	Parameter	Value	Unit
f	Working Frequency	120	kHz
V_{B_i}	Battery Voltage	3.2-4.1	V
V_B	The voltage of battery string	12.8-16.4	V
V_{SC_i}	Supercapacitor Voltage	0-7	V
$V_{\rm SC}$	The voltage of Supercapacitor string	0-28	V
C_1- C_2	Stabilizing capacitor	1000	μF
V_{DB_1}-V_{DB_4}	Voltage Drop	0.35	V
V_{DS_1}-V_{DS_4}	Voltage Drop	0.44	V
V_{SD}	Voltage Drop	0.7	V
L_1	Primary inductance	33.2	μH
L_{1mk}	Leakage of L_m	1.7	μH
L_{S_1}- L_{S_4}	Secondary Inductance	6.45	μH
L_{S_1k}- L_{S_4k}	Leakage of L_i	0.63	μH
L_2	Primary inductance	22.42	μH
L_{2mk}	Leakage of L_m	1.1	μH
L_{B_1}- L_{B_4}	Secondary Inductance	4.34	μH
L_{B_1k}- L_{B_4k}	Leakage of L_i	0.42	μH
N_1	7	-	-
N_2	2.25	-	-

P_c and P_s can be derived as

$$\begin{cases} P_c = I_{\rm in}^2 R_{DS} \\ P_s = V_S \cdot I_{\rm off} \cdot \left(\frac{E_{\rm on}+E_{\rm off}}{U_{DD} I_D} + \frac{Q_{RR}}{I_{R\_D}} \right) f \end{cases} . \tag{33}$$

When the switch turns OFF, V_S is the voltage on the switch. And $I_{\rm OFF}$ is the switch current when switching OFF.

IV. Implementation and Experimental Results

The proposed circuit for four supercapacitors and four batteries is built to verify the balance performance, as shown in Fig. 13. IRFB7437PBF MOSFETs are used for S_1 and S_2. The capacitor C is 20 μF, and the stabilizing capacitor C_1 and C_2 are 1000 μF electrolytic capacitor. DSP28335 is used to control the balance system. Table I illustrates the various parameters of the device

TABLE II
COMPARISON OF EQUALIZERS IN TERMS OF COMPONENTS

Balance methods	Component					
	MOS	Inductor	Capacitor	Diode	Transformer	Resistor
Dissipative [8]	0	0	0	0	0	8
Star-SC-Based [10]	16	0	6	0	0	0
MW-Transformer-Based [18]	16	0	0	0	2	0
matrix-Transformer-Based [16]	28	0	0	0	1	0
Half bridge-Transformer [25]	8	0	0	0	2	0
ICEBC [24]	4	2	0	20	2	0
BCI-RVM [28]	4	2	12	16	2	0
TI Bidirectional Converter [29]	4	0	12	16	2	0
Proposed equalizer	2	0	3	8	2	0

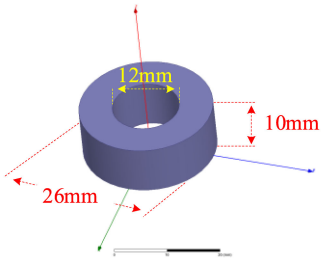

Fig. 14. Structure of the core.

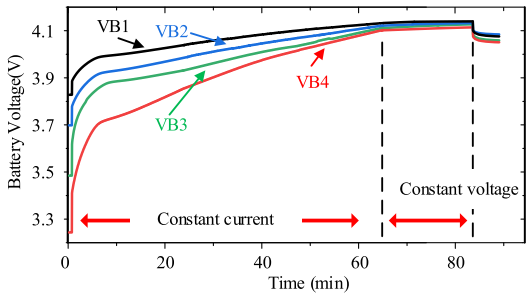

Fig. 15. Experiment verification results in the CC–CV mode.

in the circuit. The diode D_{B_i} chooses VS-30BQ015-M3/9AT (15 V and 3 A), and the diode D_{S_i} chooses SBR10U45SP5Q-13 (45 V and 10 A).

Inductors L_1 and L_2 use toroidal core, and the structure of the core is shown in Fig. 14. The cores are made by PC40.

Due to the small capacity of the supercapacitor, the power supply auxiliary supercapacitor is used to charge the battery string. The voltage change of the batteries during charging is shown in Fig. 15. The battery cells' initial voltages are 3.828, 3.699, 3.484, and 3.245 V, respectively. After about 84 min charging balance, the voltages become 4.075, 4.085, 4.063, and 4.051 V. The maximum voltage difference reduces to 0.034 V. The results show that the voltages gradually tend to be consistent.

The current ripples waveform of the multiwinding transformer M_1 and M_2 are shown in Fig. 16.

The balance current waveform of the secondary side of the multiwinding transformer M_1 is shown in Fig. 17(a). The transformer works in the forward mode, and the current flowing in the inductor L_m gradually increases when the switch S_1 is connected. The lower the voltage of the battery, the greater the balance current, which satisfies the theoretical analysis.

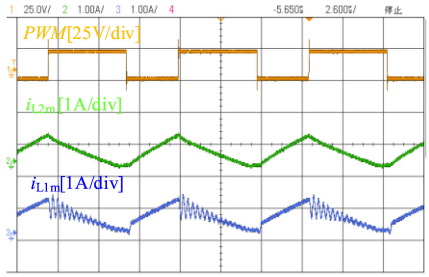

Fig. 16. Experimental waveforms of current ripples.

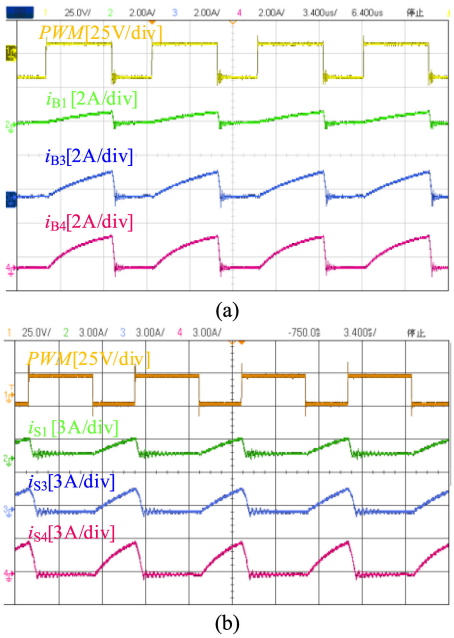

Fig. 17. The experimental waveforms of the proposed equalizer at the SSC mode.

The balance current waveform of the secondary side of the multiwinding transformer M_2 is shown in Fig. 17(b). The current flowing in the battery cells increases when the switch S_1 is turned OFF. It can be seen that the lower the voltage supercapacitor has, the greater the balance current.

When the battery string charges the supercapacitor string, the charging experiment verification results of the supercapacitor string are shown in Fig. 18. The capacity of the supercapacitor is 3F. The initial voltages of the battery cells are 2.054, 1.638,

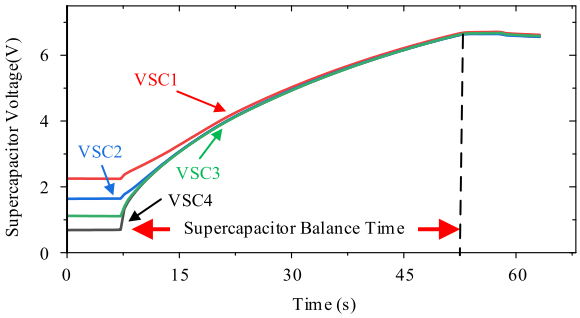

Fig. 18. Experiment verification results of four supercapacitors in charging mode.

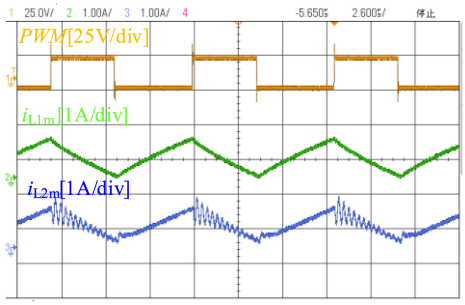

Fig. 19. Experimental waveforms of current ripples.

1.118, and 0.687 V, respectively. After about 40 s charging balance, the voltages become 6.608, 6.560, 6.567, and 6.584 V. The maximum voltage difference decreased from 1.367 to 0.048 V. The results show that the voltages gradually tend to be consistent.

The current ripples waveform of the multiwinding transformer M_1 and M_2 are shown in Fig. 19.

The balance current waveform of the secondary side of the multiwinding transformer M_2 is shown in Fig. 20(a). The transformer works in the forward mode, and the balance current flowing in supercapacitor increases when the switch S_2 is turned ON. The lower the voltage of the supercapacitor, the greater the balance current, which satisfies the theoretical analysis. The balance current waveform of the secondary side of the multiwinding transformer M_1 is shown in Fig. 20(b). The current flowing in the inductor L_m gradually increases when the switch S_2 turned OFF.

1) *In the SSC mode*

The input and output power are 18.35 and 16.73 W, respectively; hence, the system efficiency is 91.2%. The proposed system's calculated power losses are shown in Fig. 21(a), which includes internal resistance loss 0.32 W, the diode voltage drop loss 1.11 W, and switching loss 0.19 W.

2) *In the BSC mode*

The input and output power are 29.84 and 27.36 W, respectively; hence, the system efficiency is 91.7%. The proposed system's calculated power losses include internal resistance loss

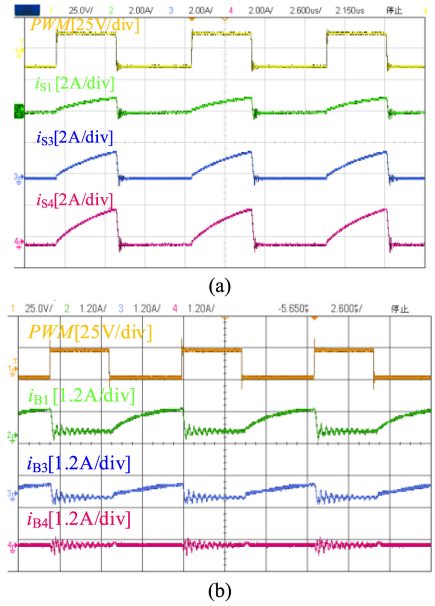

Fig. 20. The experimental waveforms of the proposed equalizer at the BSC mode.

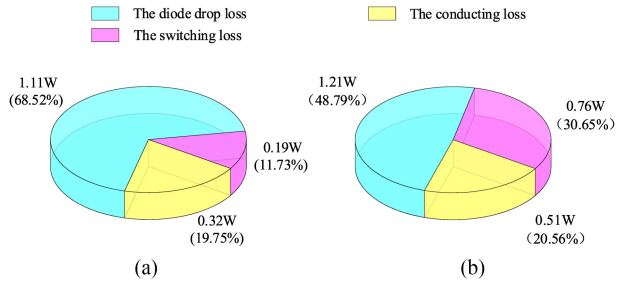

Fig. 21. Power loss distributions. (a) Supercapacitor string charging mode. (b) Battery string charging mode.

0.51 W, the diode voltage drop loss 1.21 W, and switching loss 0.76 W, as shown in Fig. 21(b).

V. Comparison With Conventional Battery Equalizers

Table II compares the proposed equalizer with the previous balance method regarding the components [12]. It is assumed that the battery string has four cells and the supercapacitor string has four cells. The circuit size and cost mainly depend on the number of components, including MOSFET (MOS), resistor, inductor, capacitor, diode, and transformer.

Table III employs four indexes to evaluate the balancing performances: balancing efficiency, cell voltage monitor, working condition, and current stress of cell. "Cell voltage monitor" refers to if the equalizer needs to collect the battery cell voltage and control the equalizer. The automatic balancing methods can achieve balance without the cell voltage monitor. "Cell current stress" refers to the current flowing through the cell.

In contrast, the proposed circuit can reduce the number of components when applied to the HESS. The proposed bidirectional equalization circuit can realize balance function in working conditions (charging or discharging).

TABLE III
COMPARISON OF BATTERY EQUALIZERS IN TERMS OF BALANCING PERFORMANCES

Balance methods	Efficiency	Cell Voltage Monitor	Working Condition	Cell Current Stress
Dissipative [8]	0.0%	No Need	Charge and Discharge	Very low
Star-SC-Based [10]	95.3%	No	Charge and Discharge	Low
MW-Transformer-Based [18]	85.3%	Yes	Charge and Discharge	Medium
matrix-Transformer-Based [16]	80.0%	Yes	Charge and Discharge	Medium
Half bridge-Transformer [25]	95%	No	Charge and Discharge	Medium
ICEBC [24]	92.4%	No	Charge	Medium
BCI-RVM [28]	72%	No	Charge and Discharge	High
TI Bidirectional Converter [29]	92.1%	No	Charge and Discharge	High
Proposed equalizer	91.2%	No	Charge and Discharge	Medium

VI. CONCLUSION

A bidirectional integrated equalizer based on the Sepic–Zeta converter is proposed for the HESS, which realizes both battery string and supercapacitor string balance during the energy exchange. The inductors in the Sepic–Zeta converter are used as the primary side of the balanced multiwinding transformer. The equalization system can realize the automatic equalization of the HESS without adding additional switches and control logic. Experimental and comparative results show that the proposed solution exhibits excellent equalization performance, while effectively reducing switches.

REFERENCES

[1] J. Nunez Forestieri and M. Farasat, "Integrative sizing/real-time energy management of a hybrid supercapacitor/undersea energy storage system for grid integration of wave energy conversion systems," *IEEE J. Emerg. Sel. Topics Power Electron.*, vol. 8, no. 4, pp. 3798–3810, Dec. 2020.

[2] Y. Ghiassi-Farrokhfal, C. Rosenberg, S. Keshav, and M.-B. Adjaho, "Joint optimal design and operation of hybrid energy storage systems," *IEEE J. Sel. Areas Commun.*, vol. 34, no. 3, pp. 639–650, Mar. 2016.

[3] B. Zakeri and S. Syri, "Electrical energy storage systems: A comparative life cycle cost analysis," *Renewable Sustain. Energy Rev.*, vol. 42, pp. 569–596, Feb. 2015.

[4] M. Uno, K. Yashiro, and K. Hasegawa, "Modularized equalization architecture with voltage multiplier-based cell equalizer and switchless switched capacitor converter-based module equalizer for series-connected electric double-layer capacitors," *IEEE Trans. Power Electron.*, vol. 34, no. 7, pp. 6356–6368, Jul. 2019.

[5] Y. Shang, N. Cui, B. Duan, and C. Zhang, "A global modular equalizer based on forward conversion for series-connected battery strings," *IEEE J. Emerg. Sel. Topics Power Electron.*, vol. 6, no. 3, pp. 1456–1469, Sep. 2018.

[6] D. F. Frost and D. A. Howey, "Completely decentralized active balancing battery management system," *IEEE Trans. Power Electron.*, vol. 33, no. 1, pp. 729–738, Jan. 2018.

[7] L. Lu, X. Han, J. Li, J. Hua, and M. Ouyang, "A review on the key issues for lithium-ion battery management in electric vehicles," *J. Power Sources*, vol. 226, pp. 272–288, 2013.

[8] J. Gallardo-Lozano *et al.*, "Battery equalization active methods," *J. Power Sources*, vol. 246, pp. 934–949, 2014.

[9] C. Pascual and P. Krein, "Switched capacitor system for automatic series battery equalization," in *Proc. IEEE Appl. Power Electron. Conf.*, 1997, pp. 848–854.

[10] Y. Shang, N. Cui, B. Duan, and C. Zhang, "Analysis and optimization of star-structured switched-capacitor equalizers for series-connected battery strings," *IEEE Trans. Power Electron*, vol. 33, no. 11, pp. 9631–9646, Nov. 2018.

[11] Y. Ye and K. W. E. Cheng, "Modeling and analysis of series–parallel switched-capacitor voltage equalizer for battery/supercapacitor strings," *IEEE Trans. Power Electron.*, vol. 3, no. 4, pp. 977–983, Dec. 2015.

[12] Y. Shang, C. Zhang, N. Cui, and C. C. Mi, "A delta-structured switched-capacitor equalizer for series-connected battery strings," *IEEE Trans. Power Electron.*, vol. 34, no. 1, pp. 452–461, Jan. 2019.

[13] Y. Yuan, K. W. E. Cheng, and Y. P. B. Yeung, "Zero-current switching switched-capacitor zero-voltage-gap automatic equalization system for series battery string," *IEEE Trans. Power Electron.*, vol. 27, no. 7, pp. 3234–3242, Jul. 2012.

[14] Y. Ye and K. W. E. Cheng, "Analysis and design of zero-current switching switched-capacitor cell balancing circuit for series-connected battery/supercapacitor," *IEEE Trans. Veh. Technol.*, vol. 67, no. 2, pp. 948–955, Feb. 2018.

[15] L. Liu, R. Mai, B. Xu, W. Sun, W. Zhou, and Z. He, "Design of parallel resonant switched-capacitor equalizer for series-connected battery strings," *IEEE Trans. Power Electron.*, vol. 36, no. 8, pp. 9160–9169, Aug. 2021.

[16] S. Lee, K. Lee, Y. Choi, and B. Kang, "Modularized design of active charge equalizer for Li-ion battery pack," *IEEE Trans. Ind. Electron.*, vol. 65, no. 11, pp. 8697–8706, Nov. 2018.

[17] M. Kim, J. Kim, and G. Moon, "Center-cell concentration structure of a cell-to-cell balancing circuit with a reduced number of switches," *IEEE Trans. Power Electron.*, vol. 29, no. 10, pp. 5285–5297, Oct. 2014.

[18] Y. Chen, X. Liu, Y. Cui, J. Zou, and S. Yang, "A multi-winding transformer cell-to-cell active equalization method for lithium-ion batteries with reduced number of driving circuits," *IEEE Trans. Power Electron.*, vol. 31, no. 7, pp. 4916–4929, Jul. 2016.

[19] Y. Shang, B. Xia, and C. Zhang, "An automatic equalizer based on forward-fly-back converter for series-connected battery strings," *IEEE Trans. Ind. Electron.*, vol. 60, no. 6, pp. 2448–2457, Jul. 2017.

[20] S. Fan, J. Duan, and L. Sun, "A fast modularized multi winding transformer balancing topology for series-connected super capacitors," *IEEE Trans. Power Electron.*, vol. 34, no. 4, pp. 3255–3268, Apr. 2019.

[21] L. Liu *et al.*, "A low-cost multiwinding transformer balancing topology for retired series-connected battery string," *IEEE Trans. Power Electron.*, vol. 36, no. 5, pp. 4931–4936, May 2021.

[22] Y. Li, J. Xu, and X. Mei, "A unitized multi winding transformer-based equalization method for series-connected battery strings," *IEEE Trans. Power Electron.*, vol. 34, no. 12, pp. 11981–11989, Dec. 2019.

[23] A. M. Imitiaz and F. H. Khan, "'Time shared fly-back converter' based regenerative cell balancing technique for series connected Li-ion battery strings," *IEEE Trans. Power Electron.*, vol. 28, no. 12, pp. 5960–5975, Dec. 2013.

[24] Y. Hsieh, T. Liang, and S. Chen, "A novel high-efficiency compact-size low-cost balancing method for series-connected battery applications," *IEEE Trans. Power Electron.*, vol. 28, no. 12, pp. 5927–5939, Dec. 2013.

[25] Y. Shang, S. Zhao, Y. Fu, B. Han, P. Hu, and C. C. Mi, "A lithium-ion battery balancing circuit based on synchronous rectification," *IEEE Trans. Power Electron.*, vol. 35, no. 2, pp. 1637–1648, Feb. 2020.

[26] M. Uno and A. Kukita, "String-to-battery voltage equalizer based on half-bridge converter with multi-stacked current doubles for series-connected batteries," *IEEE Trans. Power Electron.*, vol. 34, no. 2, pp. 1286–1298, Feb. 2018.

[27] M. Uno and K. Tanaka, "Double-switch single-transformer cell voltage equalizer using a half-bridge inverter and a voltage multiplier for series-connected supercapacitors," *IEEE Trans. Ind. Electron.*, vol. 61, no. 9, pp. 3920–3930, Nov, 2012.

[28] M. Uno and A. Kukita, "Bidirectional PWM converter integrating cell voltage equalizer using series-resonant voltage multiplier for series-connected energy storage cells," *IEEE Trans. Power Electron.*, vol. 30, no. 6, pp. 3077–3090, Jun. 2015.
[29] M. Uno and K. Yashiro, "Tapped-inductor-based single-magnetic bidirectional PWM converter integrating cell voltage equalizer for series-connected supercapacitors," *IEEE Trans. Power Electron.*, vol. 35, no. 12, pp. 13157–13171, Dec. 2020.
[30] M. Uno and K. Akio, "Single-switch single-transformer cell voltage equalizer based on forward-flyback resonant inverter and voltage multiplier for series-connected energy storage cells," *IEEE Trans. Veh. Technol.*, vol. 63, no. 9, pp. 4232–4247, Nov. 2014.
[31] M. Uno and K. Tanaka, "Single-switch multioutput charger using voltage multiplier for series-connected lithium-ion battery/supercapacitor equalization," *IEEE Trans. Ind. Electron.*, vol. 60, no. 8, pp. 3227–3239, Aug. 2013.
[32] M. Fu, C. Zhao, J. Song, and C. Ma, "A low-cost voltage equalizer based on wireless power transfer and a voltage multiplier," *IEEE Trans. Ind. Electron.*, vol. 65, no. 7, pp. 5487–5496, Jul. 2018.
[33] M. Liu, M. Fu, Y. Wang, and C. Ma, "Battery cell equalization via megahertz multiple-receiver wireless power transfer," *IEEE Trans. Power Electron.*, vol. 33, no. 5, pp. 4135–4144, May 2018.
[34] K. Lee, S. lee, Y. Choi, and B. Kang, "Active balancing of li-ion battery cells using transformer as energy carrier," *IEEE Trans. Ind. Electron.*, vol. 62, no. 2, pp. 1251–1257, Feb. 2017.
[35] Y. Shang, C. Zhang, N. Cui, and J. M. Guerrero, "A cell-to-cell battery equalizer with zero-current switching and zero-voltage gap based on quasi-resonant *LC* converter and boost converter," *IEEE Trans. Power Electron.*, vol. 30, no. 7, pp. 3731–3747, Jul. 2015.
[36] K. Lee, Y. Chung, C. Sung, and B. Kang, "Active cell balancing of li-ion batteries using *LC* series resonant circuit," *IEEE Trans. Ind. Electron.*, vol. 62, no. 9, pp. 5491–5501, Sep. 2015.

Bin Xu (Student Member, IEEE) received the B.S. degree in building electrical and intelligent engineering from the School of Urban Construction, Changchun University of Architecture, Changchun, China, in 2019. He is currently working toward the master's degree in electrical engineering with the Southwest Jiaotong University, Chengdu, China.

His research interests include battery balancing equalizers, especially on control method and circuit topology.

Zhaotian Yan received the B.Sc. degree in electrical engineering and automation from the School of Electrical Engineering, Southwest Jiaotong University, Chengdu, China, in 2018, where he is currently working toward the Ph.D. degree in electrical engineering major.

His research interest includes wireless power transfer.

Wei Zhou (Member, IEEE) received the B.E. and Ph.D. degrees in electrical engineering from the School of Automation, Chongqing University, Chongqing, China, in 2013 and 2018, respectively.

In 2016, he was a Visiting Scholar with the Department of Electrical and Computer Engineering, University of Auckland, Auckland, New Zealand. He joined the School of Electrical Engineering, Southwest Jiaotong University, Chengdu, China, as a Lecturer, in 2018. His research interests include wireless power transfer technology and its applications in rail transit system.

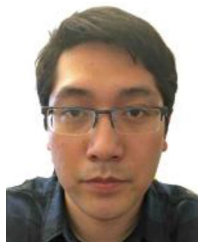

Lu Zhang received the B.S. degree in automation and the M.S. and Ph.D. degrees in computer science and engineering from Northwestern Polytechnical University, Xi'an, China, in 2012, 2015, and 2020, respectively.

From 2016 to 2018, he was a Visiting Graduate Student with the Department of Computer Science and Engineering, University of California, San Diego, CA, USA. He joined the School of Electrical Engineering, Tsinghua University, Beijing, China, as a Postdoc Researcher, in 2021. His research interests include hardware security, design automation, and embedded systems and optimization.

Huazhong Yang (Fellow, IEEE) received the B.S. degree in microelectronics and the M.S. and Ph.D. degrees in electronic engineering from the Tsinghua University, Beijing, China, in 1989, 1993, and 1998, respectively.

In 1993, he joined the Department of Electronic Engineering, Tsinghua University, where he has been a Professor since 1998. He has been in charge of several projects, including projects sponsored by the National Science and Technology Major Project, the 863 Program, NSFC, and several international research cooperations. He has authored or coauthored more than 500 technical articles, 7 books, and more than 180 granted Chinese patents. His research interests include wireless sensor networks, data converters, energy-harvesting circuits, nonvolatile processors, and brain-inspired computing.

Prof. Yang has served as a Navigating Committee Member of AsianHOST 2018 and a TPC Member of ASP-DAC 2005, APCCAS 2006, ICCCAS 2007, ASQED 2009, and ICGCS 2010. He was the recipient of the Distinguished Young Researcher by NSFC in 2000, the Cheung Kong Scholar by the Chinese Ministry of Education in 2012, the Science and Technology Award First Prize by the China Highway and Transportation Society in 2016, the Technological Invention Award First Prize by CME in 2019, the Gold Prize of iENA 2019, and several best paper awards, including ISVLSI 2012, FPGA 2017, NVMSA 2017, and ASP-DAC 2019. He has served as the Chair of the Northern China ACM SIGDA Chapter Science in 2014 and the General Co-Chair of ASP-DAC 2020.

Yongpan Liu (Senior Member, IEEE) received the B.S. degree in electrical engineering major and the M.S. degree in control engineering and Ph.D. degree in electrical engineering major from Tsinghua University, Beijing, China, in 1999, 2002, and 2007, respectively.

He is currently a tenured Full Professor with the Department of Electronic Engineering, Tsinghua University.

Prof. Liu is also a Program Committee Member of ISSCC, ASSCC, and DAC. He was the recipient of the Under 40 Young Innovators Award DAC 2017, the Best Paper/Poster Award from ASP-DAC 2021 and 2017, the Micro Top Pick 2016, HPCA 2015, and the Design Contest Awards of ISLPED in 2012, 2013, and 2019. He has served as the General Secretary for ASP-DAC 2021 and the Technical Program Chair of NVMSA 2019. He was an Associate Editor of the IEEE TRANSACTIONS ON COMPUTER-AIDED DESIGN OF INTEGRATED CIRCUITS AND SYSTEMS, the IEEE TRANSACTIONS ON CIRCUITS AND SYSTEMS II: EXPRESS BRIEFS, and the *IET Cyber-Physical Systems: Theory & Applications*. He has served as the A-SSCC2020 Tutorial Speaker and the IEEE CASS Distinguished Lecturer in 2021.

Lizhou Liu (Member, IEEE) received the B.S. degree in electrical engineering and the M.S. degree in control engineering from the Southwest University of Science and Technology, Mianyan, China, in 2014 and 2017, respectively. He is currently working toward the Ph.D. degree in electrical engineering and automation with the School of Electrical Engineering, Southwest Jiaotong University, Chengdu, China.

He joined the School of Electrical Engineering, Tsinghua University, Beijing, China, as a Lecturer, in 2022. His research interests include energy storage technology, especially battery voltage equalizer and hybrid energy storage technology.